Applying Daytime Colors to Multiband Nightvision Imagery

Alexander Toet
TNO Human Factors
Soesterberg, The Netherlands
toet@tm.tno.nl

Abstract - *We present a method to give (fused) multiband night-time imagery a natural day-time color appearance. For input, the method requires a false color RGB image that is produced by mapping 3 individual bands (or the first 3 principal components) of a multiband nightvision system to the respective channels of an RGB image. The false color RGB nightvision image is transformed into a perceptually decorrelated color space. In this color space the first order statistics of a natural color image (target scene) are transferred to the multiband nightvision image (source scene). To obtain a natural color representation of the multiband night-time imagery, the compositions of the source and target scenes should be similar to some degree. The inverse transformation to RGB space yields a nightvision image with a day-time color appearance.*

Keywords: Keywords: Image fusion, infrared, false color, nightvision, intensified imagery, pyramid.

1 Introduction

Modern night-time cameras are designed to expand the conditions under which human observers can operate. A functional piece of equipment must therefore provide an image that leads to good perceptual awareness in most environmental and operational conditions (to "Own the weather" or "Own the night"). The two most common night-time imaging systems either display emitted infrared (IR) radiation or reflected light, and thus provide complementary information of the inspected scene. A suitably combined or *fused* representation of IR and (intensified) visual imagery may enable an observer to construct a more complete mental representation of the perceived scene, resulting in a larger degree of situational awareness [17]. A false color representation of fused night-time imagery that closely resembles a natural daylight color image will help the observer by making scene interpretation more intuitive.

The rapid development of multi-band infrared and visual nightvision systems has led to an increased interest in color fused ergonomic representations of multiple sensor signals [1-3, 5, 7, 12, 13, 18-21]. Simply mapping multiple spectral bands of imagery into a three dimensional color space already generates an immediate benefit, since the human eye can discern several thousand colors, whereas it can only distinguish about 100 shades of grey at any instance. Combining bands in color space therefore provides a method to increase the dynamic range of a sensor system [4]. Experiments have convincingly demonstrated that appropriately designed false color rendering of night-time imagery can significantly improve observer performance and reaction times in tasks that involve scene segmentation and classification [5, 14, 16, 18, 24]. However, inappropriate color mappings may hinder situational awareness [8, 16, 18]. One of the main reasons seems to be the counter intuitive appearance of scenes rendered in artificial color schemes and the lack of color constancy [18]. Hence, an ergonomic color scheme should produce night vision imagery with a natural appearance and with colors that are to some extent invariant for changes in the environmental conditions (i.e. the image should always have more or less the same appearance).

Reinhard *e.a.* [10] recently introduced a method to transfer one image's color characteristics to another. The method was designed to give synthetic images a natural appearance. Here we show that this method can be applied to transfer the natural color characteristics of daylight color imagery to fused multiband nightvision images. The method employs a transformation to a principal component space that has recently been derived from a large ensemble of hyperspectral images of natural scenes [11]. In this decorrelated color space the first order statistics of natural color images (target scenes) are transferred to the multiband nightvision images (source scenes). The only requirement of the method is that the composition of the source and target scenes is similar to some extent. Hence, the depicted scenes need not be identical; they merely have to resemble each other. For surveillance systems, that usually register a fixed scene, a daylight color image of the same scene that is being

monitored can be used to derive an optimal color mapping.

Here we apply the method of Reinhard *e.a.* [10] to transfer the characteristics of natural daylight color images to false color fused night-time imagery. We demonstrate the effectiveness of the method for the combined (fused) display of visual (400-700 nm) and near infrared (700-900 nm) intensified low-light CCD images and thermal middle wavelength band (3-5 μm) infrared images. The results show that the method can be used effectively to give night-time imagery a day-time appearance. Reinhard's [10] color transfer method is in fact a simplification of a more general method that employs a principal component analysis, and that applies to any type of scene (not only to natural scenes). We show that the method can also be applied to images representing man made objects by using a full principal component analysis.

2 Imagery

A variety of outdoor scenes, displaying several kinds of vegetation (grass, heather, semi shrubs, trees), sky, water, sand, vehicles, roads, and persons, were registered at night with a recently developed dual-band visual intensified (DII) camera (see below), and with a state-of-the-art thermal middle wavelength band (3-5 μm) infrared (IR) camera (Radiance HS). Both cameras had a field of view (FOV) of about 6x6 degrees.

The DII camera was developed by Thales Optronics (Delft, The Netherlands) and facilitated a two-color registration of the scene, applying two overlapping bands covering the part of the electromagnetic spectrum ranging from visual to near infrared (400-900 nm). The short (visual) wavelength part of the incoming spectrum was mapped to the R channel of an RGB false color composite image. The long (near infrared) wavelength band corresponds primarily to the spectral reflection characteristics of vegetation, and was therefore mapped to the G channel of the RGB false color composite image. This approach utilises the fact that the spectral reflection characteristics of plants are distinctly different from other (natural and artificial) materials in the visual and near infrared range [9]. The spectral response of the long-wavelength (G) channel roughly matches that of a Generation III image intensifier system.

Images were recorded at various times of the diurnal cycle under various atmospheric conditions (clear, rain, fog, …) and for various illumination levels (1 lux – 0.1 mlux). Object ranges up to several hundreds of meters were applied. The images were digitized on-site (using a Matrox Genesis frame grabber, using at least 1.8 times oversampling).

The recorded DII and IR images were first registered through an affine warping procedure, using fiducial registration points that were recorded at the beginning of each session. After warping, corresponding pixels in images taken with the different cameras represent the same location in the recorded scene. Then, a fused false color RGB image was produced by assigning the IR image to the (empty) B channel of the false color DII image. Finally, patches displaying different types of scenic elements were selected and cut out from the resulting false color fused images. These patches were deployed as test images in the rest of this study. They display either buildings, vehicles, water, roads, trees, heather or humans. These details were selected because their signature varies strongly among the different image modalities. The false color fusion scheme results in images in which grass, trees and persons are displayed as greenish, and roads, buildings, and vehicles are brownish. Examples of the individual image modalities with their greyscale fused representation are shown in Figures 1 and 2. For brevity we can only present two different scenes here. A large number of examples with scenes of different composition are given elsewhere[15].

3 Color transfer

A variety of outdoor scenes, displaying several kinds of vegetation (grass, heather, semi shrubs, trees), sky, water, sand, vehicles, roads, and persons, were registered at night with a recently developed dual-band visual intensified (DII) camera (see below), and with a state-of-the-art thermal middle wavelength band (3-5 μm) infrared (IR) camera (Radiance HS). Both cameras had a field of view (FOV) of about 6x6 degrees.

The DII camera was developed by Thales Optronics (Delft, The Netherlands) and facilitated a two-color registration of the scene, applying two overlapping bands covering the part of the electromagnetic spectrum ranging from visual to near infrared (400-900 nm). The short (visual) wavelength part of the incoming spectrum was mapped to the R channel of an RGB false color composite image. The long (near infrared) wavelength band corresponds primarily to the spectral reflection characteristics of vegetation, and was therefore mapped to the G channel of the RGB false color composite image. This approach utilises the fact that the spectral reflection characteristics of plants are distinctly different from other (natural and artificial) materials in the visual and near infrared range [9]. The spectral response of the long-wavelength (G) channel roughly matches that of a Generation III image intensifier system.

Images were recorded at various times of the diurnal cycle under various atmospheric conditions (clear, rain, fog, …) and for various illumination levels (1 lux – 0.1 mlux). Object ranges up to several hundreds of meters

were applied. The images were digitized on-site (using a Matrox Genesis frame grabber, using at least 1.8 times oversampling).

The recorded DII and IR images were first registered through an affine warping procedure, using fiducial registration points that were recorded at the beginning of each session. After warping, corresponding pixels in images taken with the different cameras represent the same location in the recorded scene. Then, a fused false color RGB image was produced by assigning the IR image to the (empty) B channel of the false color DII image. Finally, patches displaying different types of scenic elements were selected and cut out from the resulting false color fused images. These patches were deployed as test images in the rest of this study. They display either buildings, vehicles, water, roads, trees, heather or humans. These details were selected because their signature varies strongly among the different image modalities. The false color fusion scheme results in images in which grass, trees and persons are displayed as greenish, and roads, buildings, and vehicles are brownish. Examples of the individual image modalities with their greyscale fused representation are shown in Figures 1 and 2. For brevity we can only present two different scenes here. A large number of examples with scenes of different composition are given elsewhere [15].

3.1 RGB to *LMS* transform

First the RGB tristimulus values are converted to device independent XYZ tristimulus values. This conversion depends on the characteristics of the display on which the image was originally intended to be displayed. Because that information is rarely available, it is common practice to use a device-independent conversion that maps white in the chromaticity diagram to white in RGB space and vice versa [6].

$$\begin{bmatrix} X \\ Y \\ Z \end{bmatrix} = \begin{bmatrix} 0.5141 & 0.3239 & 0.1604 \\ 0.2651 & 0.6702 & 0.0641 \\ 0.0241 & 0.1228 & 0.8444 \end{bmatrix} \begin{bmatrix} R \\ G \\ B \end{bmatrix} \quad (1)$$

The device independent XYZ values are then converted to LMS space by

$$\begin{bmatrix} L \\ M \\ S \end{bmatrix} = \begin{bmatrix} 0.3897 & 0.6890 & -0.0787 \\ -0.2298 & 1.1834 & 0.0464 \\ 0.0000 & 0.0000 & 1.0000 \end{bmatrix} \begin{bmatrix} X \\ Y \\ Z \end{bmatrix} \quad (2)$$

Combination of (1) and (2) results in

$$\begin{bmatrix} L \\ M \\ S \end{bmatrix} = \begin{bmatrix} 0.3811 & 0.5783 & 0.0402 \\ 0.1967 & 0.7244 & 0.0782 \\ 0.0241 & 0.1288 & 0.8444 \end{bmatrix} \begin{bmatrix} R \\ G \\ B \end{bmatrix} \quad (3)$$

The data in this color space shows a great deal of skew, which is largely eliminated by taking a logarithmic transform:

$$\begin{aligned} \boldsymbol{L} &= \log L \\ \boldsymbol{M} &= \log M \\ \boldsymbol{S} &= \log S \end{aligned} \quad (4)$$

The inverse transform from ***LMS*** cone space back to RGB space is as follows. First, the ***LMS*** pixel values are raised to the power ten to go back to linear LMS space. Then, the data can be converted from LMS to RGB using the inverse transform of Equation (3):

$$\begin{bmatrix} R \\ G \\ B \end{bmatrix} = \begin{bmatrix} 4.4679 & -3.5873 & 0.1193 \\ -1.2186 & 2.3809 & -0.1624 \\ 0.0497 & -0.2439 & 1.2045 \end{bmatrix} \begin{bmatrix} L \\ M \\ S \end{bmatrix} \quad (5)$$

3.2 Transfer Method I: principal component transform

The principal component transform effectively rotates the ***LMS*** coordinate axes such that the pixel components are maximally decorrelated. The set of normalized eigenvectors of the covariance matrix of the set of pixel values, arranged in order of increasing eigenvalues, constitute the column vectors of the corresponding rotation matrix. Let R_t be the rotation matrix that decorrelates the target pixels. The pixel values of the source and target images in this new coordinate system are then respectively given by

$$\begin{bmatrix} \boldsymbol{L}_s' \\ \boldsymbol{M}_s' \\ \boldsymbol{S}_s' \end{bmatrix} = R_t \begin{bmatrix} \boldsymbol{L}_s \\ \boldsymbol{M}_s \\ \boldsymbol{S}_s \end{bmatrix} \quad (6)$$

and

$$\begin{bmatrix} \boldsymbol{L}_t' \\ \boldsymbol{M}_t' \\ \boldsymbol{S}_t' \end{bmatrix} = R_t \begin{bmatrix} \boldsymbol{L}_t \\ \boldsymbol{M}_t \\ \boldsymbol{S}_t \end{bmatrix} \quad (7)$$

where the indices *s* and *t* refer to the source and target images respectively.

First, the mean is subtracted from the data points:

$$\begin{aligned} \boldsymbol{L}^* &= \boldsymbol{L}' - \langle \boldsymbol{L}' \rangle \\ \boldsymbol{M}^* &= \boldsymbol{M}' - \langle \boldsymbol{M}' \rangle \\ \boldsymbol{S}^* &= \boldsymbol{S}' - \langle \boldsymbol{S}' \rangle \end{aligned} \quad (8)$$

Then, the source data points are scaled with the ratio of the standard deviations of the source and target images respectively:

$$\begin{aligned} \boldsymbol{L}_s^+ &= \frac{\sigma_t^{\boldsymbol{L}}}{\sigma_s^{\boldsymbol{L}}} \boldsymbol{L}_s^* \\ \boldsymbol{M}_s^+ &= \frac{\sigma_t^{\boldsymbol{M}}}{\sigma_s^{\boldsymbol{M}}} \boldsymbol{M}_s^* \\ \boldsymbol{S}_s^+ &= \frac{\sigma_t^{\boldsymbol{S}}}{\sigma_s^{\boldsymbol{S}}} \boldsymbol{S}_s^* \end{aligned} \qquad (9)$$

After this transformation, the resulting data points have standard deviations that correspond to those of the target image. Before reconstructing the RGB representation the averages computed over the target image are added to the source image:

$$\begin{aligned} \boldsymbol{L}_s^\oplus &= \boldsymbol{L}_s^+ + \langle \boldsymbol{L}_t' \rangle \\ \boldsymbol{M}_s^\oplus &= \boldsymbol{M}_s^+ + \langle \boldsymbol{M}_t' \rangle \\ \boldsymbol{S}_s^\oplus &= \boldsymbol{S}_s^+ + \langle \boldsymbol{S}_t' \rangle \end{aligned} \qquad (10)$$

After this transformation, the mean and standard deviation of the source image conform to those of the target image. The result is transformed back to RGB space via the inverse rotation R_t^{-1}, logLMS, LMS, and XYZ color space using Equation (5).

3.3 Transfer Method II: *lαβ* transform

Ruderman *e.a.* [11] recently derived a color space, called *lαβ*, which effectively minimises the correlation between the ***LMS*** axes. This result was derived from a principal component transform to the logarithmic ***LMS*** cone space representation of a large ensemble of hyperspectral images that represented a good cross-section of natural scenes. The principal axes encode fluctuations along an achromatic direction (*l*), a yellow-blue opponent direction (*α*), and a red-green opponent direction (*β*). The resulting data representation is compact and symmetrical, and provides automatic decorrelation to higher than second order.

Ruderman *e.a.* [11] presented the following simple transform to decorrelate the axes in the ***LMS*** space:

$$\begin{bmatrix} l \\ \alpha \\ \beta \end{bmatrix} = \begin{bmatrix} \frac{1}{\sqrt{3}} & 0 & 0 \\ 0 & \frac{1}{\sqrt{6}} & 0 \\ 0 & 0 & \frac{1}{\sqrt{2}} \end{bmatrix} \begin{bmatrix} 1 & 1 & 1 \\ 1 & 1 & -2 \\ 1 & -1 & 0 \end{bmatrix} \begin{bmatrix} \boldsymbol{L} \\ \boldsymbol{M} \\ \boldsymbol{S} \end{bmatrix} \qquad (11)$$

If we think of the **L** channel as red, the **M** as green, and **S** as blue, we see that this is a variant of a color opponent model:

$$\begin{aligned} \text{Achromatic} &\propto r+g+b \\ \text{Yellow-blue} &\propto r+g-b \\ \text{Red-green} &\propto r-g \end{aligned} \qquad (12)$$

After processing the color signals in the $l\alpha\beta$ space the inverse transform of Equation (11) can be used to return to the ***LMS*** space:

$$\begin{bmatrix} \boldsymbol{L} \\ \boldsymbol{M} \\ \boldsymbol{S} \end{bmatrix} = \begin{bmatrix} 1 & 1 & 1 \\ 1 & 1 & -1 \\ 1 & -2 & 0 \end{bmatrix} \begin{bmatrix} \frac{\sqrt{3}}{3} & 0 & 0 \\ 0 & \frac{\sqrt{6}}{6} & 0 \\ 0 & 0 & \frac{\sqrt{2}}{2} \end{bmatrix} \begin{bmatrix} l \\ \alpha \\ \beta \end{bmatrix} \qquad (13)$$

The processing in the $l\alpha\beta$ space is similar to the processing applied in the previous section, and given by Equations (8)--(10). First, mean is subtracted from the source and target data points:

$$\begin{aligned} l^* &= l - \langle l \rangle \\ \alpha^* &= \alpha - \langle \alpha \rangle \\ \beta^* &= \beta - \langle \beta \rangle \end{aligned} \qquad (14)$$

Then, the source data points are scaled with the ratio of the standard deviations of the source and target images respectively:

$$\begin{aligned} l_s' &= \frac{\sigma_t^l}{\sigma_s^l} l_s^* \\ \alpha_s' &= \frac{\sigma_t^\alpha}{\sigma_s^\alpha} \alpha_s^* \\ \beta_s' &= \frac{\sigma_t^\beta}{\sigma_s^\beta} \beta_s^* \end{aligned} \qquad (15)$$

After this transformation the pixels comprising the multiband source image have standard deviations that conform to the target daylight color image. Finally, in reconstructing the $l\alpha\beta$ transform of the multiband source image, instead of adding the previously subtracted averages, the averages computed for the target daylight color image are added. The result is transformed back to RGB space via logLMS, LMS, and XYZ color space using Equations (13) and (5).

4 Example

Figure 1 shows night-time images of a rural scene taken with respectively (1a) the visual (400-700 nm) and (1b) the near infrared (700-900 nm) bands of a double-band image intensifier, and (1c) a 3-5 μm midwave infrared camera. The graylevel fused combination of the three images is also shown (1d).

Figure 2 illustrates the application of colour transfer Method I to the false colour RGB source images obtained by mapping respectively the visual (400-700 nm) and the near infrared (700-900 nm) intensified low-light CCD images and the thermal middle wavelength band (3-5 μm) infrared images from Figure 1 to respectively the R, G, and B bands of a false colour representation (top). Results are shown for a number of different target images (left row). The first target image in these examples (top left row) is a daylight colour photograph of the same scene that is represented on top as a false colour RGB image, and that was recorded at night in full darkness with both the dual-band image intensifier and the thermal middle wavelength infrared camera. The colour in these target photographs is somewhat washed out because of atmospheric attenuation, since the viewing distance was about 800 m. Note that the colour of the target photograph returns in the processed false colour night-time imagery (top right column). Hence, the colour transfer method is effective in giving night-time imagery a day-time appearance. The results produced with Methods I and II are quite similar (for reasons of brevity not shown here, for an extensive comparison of both methods see [15]). This implies that for the type of imagery we investigated in this study the costly principal component analysis of Method I can be replaced by the simple matrix transform of Method II.

Figure 2 also demonstrate the fact that the actual choice of the target image is not critical, as long as the colour distribution is to some extent similar to that of the source scene. The left column shows the different target images used in the colour transfer Method I. The right column represents the result of applying the colour transfer Method I to the image on top with the corresponding image in the left column as the target. The results show that the appearance of the final result resembles that of the target image in each case.

Figure 2 also shows an example (5th row) in which an oil painting called “Old Oak Tree”, by the Dutch painter Barend Cornelius Koekkoek (1803-1862), was adopted as the target image. The corresponding result has an appearance which is quite natural. However, the example shown in the 4th row of Figure 15 shows that the method fails when the colour composition of the target and the source images are too dissimilar. In this case, the target image displays green grass and green trees with a bright blue sky in the background. The source image in contrast only shows brownish trees and vegetation. As a result, the transfer of statistics fails in this case.

(a)

(b)

(c)

(d)

Figure 1 Night-time images of a scene representing a sandy path, trees, and fences, and taken with respectively (a) the visual (400-700 nm) and (b) the near infrared (700-900 nm) bands of a double-band image intensifier, and (c) a 3-5 μm midwave infrared camera. (d) The graylevel fused combination of the three images (a-c).

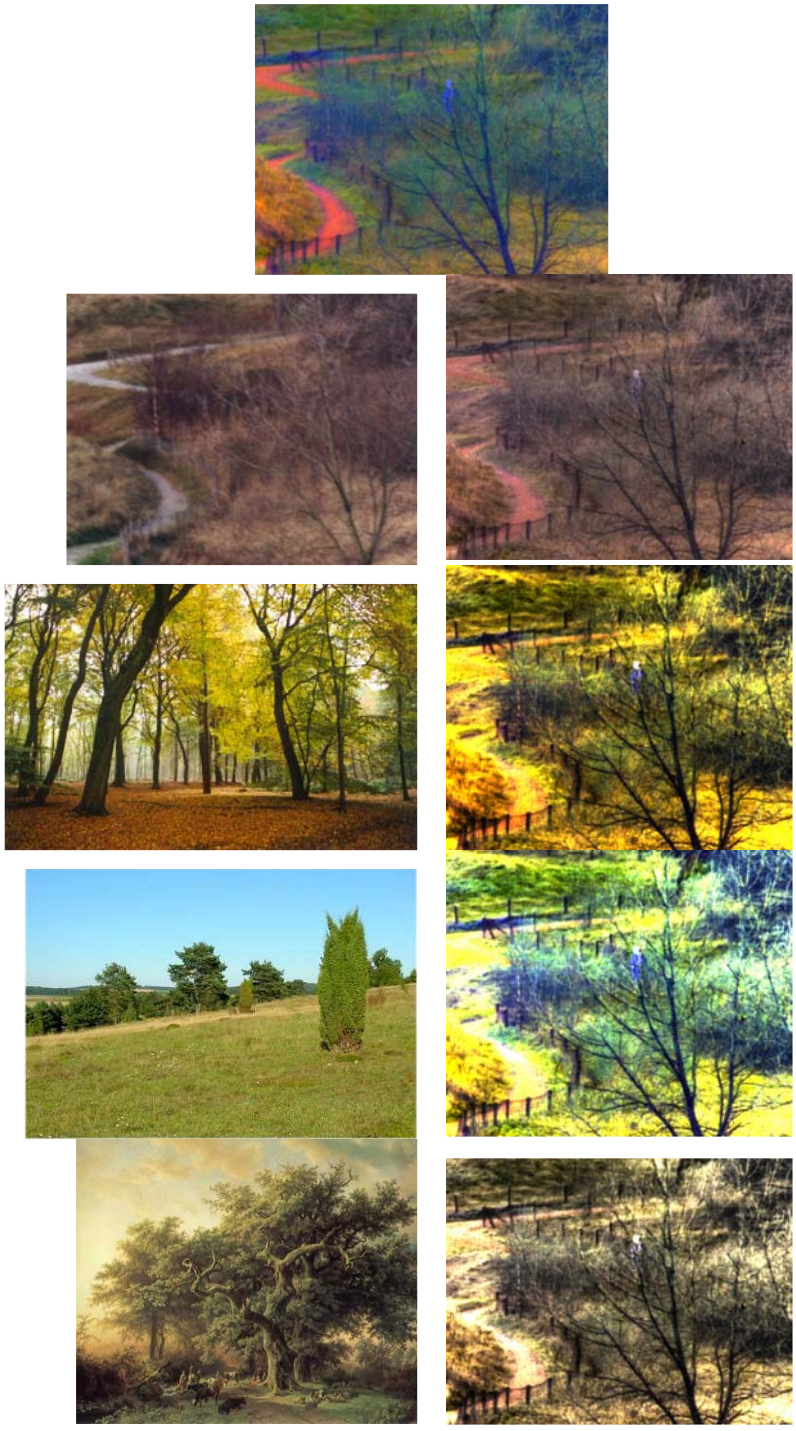

Figure 2 Illustration of colour transfer Method I and the use of different target images. Top: False colour image obtained by mapping respectively the images a, b and c from Figure 1 to the R, G and B channels of an RGB colour image. Notice the unnatural appearance of this image. Left column: the different target images. Right column: the corresponding results of the colour transfer. The top image in the left column is a daylight photograph of the same scene (but without the person). The lower left target image is a painting called “Old Oak Tree”, by the Dutch master Barend Cornelius Koekkoek (1803-1862). Notice the resemblance between the colour characteristics of the results of the colour mapping (right column) and the target images (left column).

5 Concluding remarks

We showed that a recently introduced method to transfer one image's color characteristics to another [10] can be used effectively to give multiband night-time imagery a natural day-time color appearance. The contrast of the resulting color imagery can be improved by mapping a grayscale fused representation of the individual image bands to the luminance component of the resulting color images. The color transfer method presented here can also be applied to remap the color distribution of imagery resulting from existing color fusion methods [1-3, 5, 7, 12, 13, 18-23]. A large number of full color examples with scenes of different composition is given elsewhere [15].

The color transfer method employs a transformation to a principal component space. In this decorrelated color space the first order statistics of natural color images (target scenes) are transferred to the multiband nightvision images (source scenes). We applied the method to a set of RGB false color night-time images recorded both with a dual band (visual and near infrared) image intensified low-light CCD camera (DII) and with a thermal middle wavelength band (3-5 μm) infrared (IR) camera. In each case, the resulting false color night-time images adopted the appearance of the day-time color images of the corresponding scene.

In this study we applied the method to source images with two or three spectral bands. When the input multiband image has more than three bands the method can also be applied. In that case a false color RGB source image can be constructed by mapping the first three principal components of the multiband input image to the three channels of the RGB image. The color mapping can then be applied to this false color source image.

The color transfer method only uses the first order statistics of natural color images that are representative of the depicted scene. This implies that only 6 numbers (the three components of respectively the mean and standard deviation of the image components in ***LMS*** cone space) are required to apply a natural day-time color appearance to multiband night-time imagery. Hence, there is no need to actually store the target images from which the color information (the first order statistics) is derived. A system that is equipped with a look-up table of characteristic numbers for different types of backgrounds is sufficient to enable the observer to adjust the color mapping to the scene being viewed.

Night-time images recorded with an intensified low-light CCD camera and a thermal middle wavelength band (3-5 μm) infrared camera contain *complementary* information. This makes each of the individual image modalities only suited for specific observation tasks. In many operational conditions different nightvision systems are used side by side. By using a combined or fused display method the complementarity of the information in the image modalities can be fully exploited, thus enabling multiple observation tasks to be performed with a single night-time image representation. A full color representation of night-time scenes may be of great ergonomic value by making the interpretation (segmentation) of the displayed scene easier (more intuitive) for the observer.

Since there evidently exists no one-to-one mapping between the temperature contrast and the spectral reflectance of a material, the goal of producing a night-time image, incorporating information from IR imagery, with an appearance identical to a color day-time image can never be fully achieved. The method employed here allows one *(1)* to settle for a single mapping that works satisfactorily in a large number of conditions (e.g. by selecting the color statistics of a generic representative scene), or *(2)* to adapt (optimise) the color mapping to the situation at hand (e.g. by selecting the color statistics that perfectly match the scene at hand).

Acknowledgements

This work was supported by the European Office of Aerospace Research and Development, Air Force Office of Scientific Research, Air Force Research Laboratory, under contract No. F61775-01-WE026, and by Senter, Agency of the Ministry of Economic Affairs of the Netherlands

References

[1] Aguilar, M., Fay, D.A., Ireland, D.B., Racamoto, J.P., Ross, W.D. & Waxman, A.M. (1999). Field evaluations of dual-band fusion for color night vision. In J.G. Verly (Ed.), *Enhanced and Synthetic Vision 1999* (pp. 168-175). Bellingham, WA: The International Society for Optical Engineering.

[2] Aguilar, M., Fay, D.A., Ross, W.D., Waxman, A.M., Ireland, D.B. & Racamoto, J.P. (1998). Real-time fusion of low-light CCD and uncooled IR imagery for color night vision. In J.G. Verly (Ed.), *Enhanced and Synthetic Vision 1998* (pp. 124-135). Bellingham, WA: The International Society for Optical Engineering.

[3] Aguilar, M. & Garret, A.L. (2001). Biologically based sensor fusion for medical imaging. In B.V. Dasarathy (Ed.), *Sensor Fusion: Architectures, Algorithms, and Applications V* (pp. 149-158). Bellingham, WA: The International Society for Optical Engineering.

[4] Driggers, R.G., Krapels, K.A., Vollmerhausen, R.H., Warren, P.R., Scribner, D.A., Howard, J.G., Tsou, B.H. & Krebs, W.K. (2001). Target detection threshold in noisy color imagery. In G.C. Holst (Ed.), *Infrared Imaging Systems: Design, Analysis, Modeling, and Testing XII* (pp. 162-169). Bellingham, WA: The International Society for Optical Engineering.

[5] Essock, E.A., Sinai, M.J., McCarley, J.S., Krebs, W.K. & DeFord, J.K. (1999). Perceptual ability with real-world nighttime scenes: image-intensified, infrared, and fused-color imagery. *Human Factors, 41(3),* 438-452.

[6] Fairchild, M.D. (1998). *Color appearance models.* Reading, MA: Addison Wesley Longman, Inc.

[7] Fay, D.A., Waxman, A.M., Aguilar, M., Ireland, D.B., Racamato, J.P., Ross, W.D., Streilein, W. & Braun, M.I. (2000). Fusion of multi-sensor imagery for night vision: color visualization, target learning and search.*Proceedings of the 3rd International Conference on Information Fusion* (pp. TuD3-3-TuD3-10). Paris, France: ONERA.

[8] Krebs, W.K., Scribner, D.A., Miller, G.M., Ogawa, J.S. & Schuler, J. (1998). Beyond third generation: a sensor-fusion targeting FLIR pod for the F/A-18. In B.V. Dasarathy (Ed.), *Sensor Fusion: Architectures, Algorithms, and Applications II* (pp. 129-140). Bellingham, WA, USA: International Society for Optical Engineering.

[9] Onyango, C.M. & Marchant, J.A. (2001). Physics-based colour image segmentation for scenes containing vegetation and soil. *Image and Vision Computing, 19(8),* 523-538.

[10] Reinhard, E., Ashikhmin, M., Gooch, B. & Shirley, P. (2001). Color transfer between images. *IEEE Computer Graphics and Applications, 21(5),* 34-41.

[11] Ruderman, D.L., Cronin, T.W. & Chiao, C.-C. (1998). Statistics of cone responses to natural images: implications for visual coding. *Journal of the Optical Society of America A, 15(8),* 2036-2045.

[12] Schuler, J., Howard, J.G., Warren, P., Scribner, D.A., Klien, R., Satyshur, M. & Kruer, M.R. (2000). Multiband E/O color fusion with consideration of noise and registration. In W.R. Watkins, D. Clement & W.R. Reynolds (Ed.), *Targets and Backgrounds VI: Characterization, Visualization, and the Detection Process* (pp. 32-40). Bellingham, WA, USA: The International Society for Optical Engineering.

[13] Scribner, D.A., Warren, P. & Schuler, J. (1999). Extending color vision methods to bands beyond the visible.*Proceedings of the IEEE Workshop on Computer Vision Beyond the Visible Spectrum: Methods and Applications* (pp. 33-40).Institute of Electrical and Electronics Engineers.

[14] Sinai, M.J., McCarley, J.S., Krebs, W.K. & Essock, E.A. (1999). Psychophysical comparisons of single- and dual-band fused imagery. In J.G. Verly (Ed.), *Enhanced and Synthetic Vision 1999* (pp. 176-183). Bellingham, WA: The International Society for Optical Engineering.

[15] Toet, A. (2002). *Paint the night: applying daylight colours to nighttime imagery* (Report TM-02-B006). Soesterberg, The Netherlands: TNO Human Factors.

[16] Toet, A. & IJspeert, J.K. (2001). Perceptual evaluation of different image fusion schemes. In I. Kadar (Ed.), *Signal Processing, Sensor Fusion, and Target Recognition X* (pp. 436-441). Bellingham, WA: The International Society for Optical Engineering.

[17] Toet, A., IJspeert, J.K., Waxman, A.M. & Aguilar, M. (1998). Fusion of visible and thermal imagery improves situational awareness. *Displays, 18,* 85-95.

[18] Varga, J.T. (1999). *Evaluation of operator performance using true color and artificial color in natural scene perception* (Report AD-A363036). Monterey, CA: Naval Postgraduate School.

[19] Waxman, A.M., Aguilar, M., Baxter, R.A., Fay, D.A., Ireland, D.B., Racamoto, J.P. & Ross, W.D. (1998). Opponent-color fusion of multi-sensor imagery: visible, IR and SAR.*Proceedings of the 1998 Conference of the IRIS Specialty Group on Passive Sensors* (pp. 43-61).

[20] Waxman, A.M., et al. (1999). Solid-state color night vision: fusion of low-light visible and thermal infrared imagery. *MIT Lincoln Laboratory Journal, 11,* 41-60.

[21] Waxman, A.M., Carrick, J.E., Fay, D.A., Racamato, J.P., Augilar, M. & Savoye, E.D. (1996). Electronic imaging aids for night driving: low-light CCD, thermal IR, and color fused visible/IR.*Proceedings of the SPIE Conference on Transportation Sensors and Controls* Bellingham, WA: The International Society for Optical Engineering.

[22] Waxman, A.M., Fay, D.A., Gove, A.N., Seibert, M.C., Racamato, J.P., Carrick, J.E. & Savoye, E.D. (1995). Color night vision: fusion of intensified visible and thermal IR imagery. In J.G. Verly (Ed.), *Synthetic Vision for Vehicle Guidance and Control* (pp. 58-68). Bellingham, WA: The International Society for Optical Engineering.

[23] Waxman, A.M., Gove, A.N., Fay, D.A., Racamoto, J.P., Carrick, J.E., Seibert, M.C. & Savoye, E.D. (1997). Color night vision: opponent processing in the fusion of visible and IR imagery. *Neural Networks, 10(1),* 1-6.

[24] White, B.L. (1998). *Evaluation of the impact of multispectral image fusion on human performance in global scene processing* (Report AD-A343639). Monterey, CA: Naval Postgraduate School.